www.MaterialsViews.com

Metabolizable Ultrathin Bi_2Se_3 Nanosheets in Imaging-Guided Photothermal Therapy

Hanhan Xie, Zhibin Li, Zhengbo Sun, Jundong Shao, Xue-Feng Yu, Zhinan Guo, Jiahong Wang, Quanlan Xiao, Huaiyu Wang, Qu-Quan Wang,* Han Zhang, and Paul K. Chu**

***P**oly(vinylpyrrolidone)-encapsulated Bi_2Se_3 nanosheets with a thickness of 1.7 nm and diameter of 31.4 nm are prepared by a solution method. Possessing an extinction coefficient of 11.5 L g^{-1} cm^{-1} at 808 nm, the ultrathin Bi_2Se_3 nanosheets boast a high photothermal conversion efficiency of 34.6% and excellent photoacoustic performance. After systemic administration, the Bi_2Se_3 nanosheets with the proper size and surface properties accumulate passively in tumors enabling efficient photoacoustic imaging of the entire tumors to facilitate photothermal cancer therapy. In vivo biodistribution studies reveal that they are expelled from the body efficiently after 30 d. The ultrathin Bi_2Se_3 nanosheets have large clinical potential as metabolizable near-infrared-triggered theranostic agents.*

Dr. H. Xie, Dr. Z. Li, Prof. X.-F. Yu, Prof. H. Wang
Institute of Biomedicine and Biotechnology
Shenzhen Institutes of Advanced Technology
Chinese Academy of Sciences
Shenzhen 518055, P. R. China
E-mail: xf.yu@siat.ac.cn

Dr. H. Xie, Dr. J. Wang, Prof. Q.-Q. Wang
Department of Physics
Wuhan University
Wuhan 430072, P. R. China
E-mail: qqwang@whu.edu.cn

Dr. Z. Sun, Dr. J. Shao, Dr. Z. Guo, Dr. Q. Xiao, Prof. H. Zhang
SZU-NUS Collaborative Innovation Center for Optoelectronic Science and Technology
Key Laboratory of Optoelectronic Devices and Systems of Ministry of Education and Guangdong Province
College of Optoelectronic Engineering
Shenzhen University
Shenzhen 518060, P. R. China

Prof. H. Wang, Prof. P. K. Chu
Department of Physics and Materials Science
City University of Hong Kong
Tat Chee Avenue
Kowloon, Hong Kong 999077, China
E-mail: paul.chu@cityu.edu.hk

DOI: 10.1002/smll.201601050

1. Introduction

Photothermal (PT) therapy based on tissue-transparent near-infrared (NIR) light has been gaining clinical acceptance in cancer treatment due to the specific spatial/temporal selectivity and minimal invasiveness.[1,2] Various inorganic nanoparticles with excellent NIR optical properties have been explored as nanoagents in PT therapy.[3–9] Compared to small molecules, nanoparticles with the proper size (usually 10–50 nm) can accumulate passively in tumors at higher concentrations as a result of the enhanced permeability and retention (EPR) effect.[10,11] In addition, some nanoparticles with multiple functionalities enable imaging-guided PT therapy thereby promoting the treatment precision of cancer and mitigating undesired side effects.[12–19] However, unlike small molecules which usually can be rapidly excreted from the body after systemic administration, inorganic nanoparticles generally have poor metabolizability and their potential long-term toxicity is a serious concern hampering clinical acceptance. To be clinically viable, the PT agent should have the following properties: (1) excellent NIR optical performance enabling highly efficient PT therapy, (2) proper size enabling efficient accumulation in tumors, and (3) good biocompatibility and clearance from the body within a reasonable time.

In recent years, 2D layered materials such as graphene and transition-metal dichalcogenides have attracted much

attention due to their unique properties and promising applications to many areas including nanomedicine.[20–30] As a class of 2D layered topological insulators, bismuth selenide (Bi_2Se_3) has remarkable thermoelectric and photoelectric properties[31–34] and is attractive to biomedicine due to the good bioactivity and biocompatibility. Bi is an environmentally friendly element and has been widely used in X-ray contrast agents due to the large atomic number and photoelectric absorption coefficient[35–37] and Se is an essential trace element with a recommended dietary allowance of 55 mg d^{-1}.[38] Jeong and co-workers have synthesized spiral-type Bi_2Se_3 nanosheets with 4–6 quantum layers (QLs) and lateral diameter between 50 and 100 nm[39] and they are the smallest Bi_2Se_3 nanosheets up to data with biomedical potential.[25,26] From the perspective of efficient excretion from the body after systemic administration, smaller Bi_2Se_3 nanosheets are desirable. Furthermore, Bi_2Se_3 with a thickness down to few quantum layers (1–2 QLs) is expected to possess improved optical absorption properties.[40]

In this work, ultrathin Bi_2Se_3 nanosheets with a thickness of only 1.7 nm (≈2 QLs) and diameter of 31.4 nm are synthesized and applied to photoacoustic (PA) imaging-guided PT therapy of cancer. After systemic administration, they accumulate passively in tumors enabling PA imaging-guided PT therapy and are expelled from the body in one month.

2. Results and Discussion

2.1. Synthesis and Characterization of the Poly(vinylpyrrolidone) (PVP)-Encapsulated Bi_2Se_3 Nanosheets

The Bi_2Se_3 nanosheets were prepared by a simple solution-based method using PVP as a surfactant. In a standard synthesis, a NaHSe solution was produced by reacting $NaBH_4$ with Se powders in an ice-water bath. The reaction took place in ethylene glycol (EG) mixed with $Bi(NO_3)_3$ and PVP at 160 °C under N_2. The freshly synthesized oxygen-free NaHSe solution was rapidly injected to the mixture by a syringe and the mixture turned dark immediately due to formation of PVP-encapsulated Bi_2Se_3 nanosheets. More details about the synthesis can be found in the Experimental Section. In previously reported solution-based methods to synthesize Bi_2Se_3, Na_2SeO_3 is generally required as the Se source but it is toxic. In contrast, the reagents used here such as Se powders and NaHSe are much safer.

To investigate the growth mechanism of the Bi_2Se_3 nanosheets, a small amount of the reaction solution was transferred to a cold glass bottle and kept in an ice bath to quench the reaction. The products were collected and washed at least three times. The formation process of the Bi_2Se_3 nanosheets is presented in Figure S1 in the Supporting Information schematically. After rapid injection of the NaHSe solution into the reaction medium at 160 °C, the solution became dark immediately. In the initial stage (t = 3 s, Figure S1a, Supporting Information), the Bi_2Se_3 particles with an amorphous structure were obtained and these particles aggregated later (t = 8 s, Figure S1b, Supporting Information), followed by the formation of an incipient nanosheet as the reaction continued (t = 15 s, Figure S1c, Supporting Information). The nanosheet further developed into a mature Bi_2Se_3 nanosheet when the reaction time was extended to t = 1 min (Figure S1d, Supporting Information).

The morphology of the Bi_2Se_3 nanosheets is examined by transmission electron microscopy (TEM) and atomic force microscopy (AFM). Based on the TEM images in **Figure 1**a,b, the Bi_2Se_3 nanosheets have a relatively uniform size with an average diameter of 31.4 ± 5.3 nm (Figure 1d). The high-resolution TEM (HR-TEM) image in Figure 1c shows clear lattice fringes of 0.208 nm ascribed to the (110) plane of the Bi_2Se_3 crystal.[25] The AFM image in Figure 1f shows heights of 2.2, 1.3, 1.4, and 1.2 nm, respectively (Figure 1g,h). The average thickness is 1.7 ± 0.6 nm corresponding to a stack of ≈2 QLs of Bi_2Se_3 according to the statistical AFM analysis (Figure 1i). Compared to previously reported Bi_2Se_3 nanosheets, nanoribbons, and nanoplates, the Bi_2Se_3 nanosheets here are the thinnest and smallest.

The Bi_2Se_3 nanosheets are characterized by powder X-ray diffraction (XRD). As shown in Figure 1e, all the peaks can be indexed to the rhombohedral phase of Bi_2Se_3.[41] Elemental analysis is performed by energy-dispersive X-ray spectrometry (EDS) and Figure 1j reveals that Bi and Se are uniformly distributed with a stoichiometric ratio of 2:3. The Bi_2Se_3 nanosheets are also characterized by Raman scattering (Figure S2, Supporting Information). The Eg^2 (in-plane) and $A_{1g}{}^2$ (out-of-plane) modes are observed at 125 and 170 cm^{-1}, respectively. Compared to bulk Bi_2Se_3, the Eg^2 and $A_{1g}{}^2$ modes of the Bi_2Se_3 nanosheets redshift by ≈5 and 3 cm^{-1}, respectively, mainly due to phonon softening.[42] The chemical composition of the Bi_2Se_3 nanosheets is determined by X-ray photoelectron spectroscopy (XPS). The XPS survey spectrum is presented in Figure S3a in the Supporting Information where shows Bi, Se, C, and O only. The two peaks in Figure S3b in the Supporting Information corresponding to the Bi $4f_{5/2}$ and $4f_{7/2}$ peaks are observed at 158.6 and 164.0 eV, respectively. The high-resolution spectrum of Se 3d in Figure S3c in the Supporting Information shows the peaks at around 53.1 eV (Se $3d_{5/2}$) and 54.8 eV (Se $3d_{3/2}$). Furthermore, there is a peak at around 57.9 eV corresponding to oxidized selenium (i.e., SeO_x) which has been observed previously.[43]

As a nontoxic and widely used stabilizing agent in biomedical applications, PVP is employed as a surfactant to stabilize the reaction and functionalize the particle surface. Fourier transform infrared (FTIR) is generally used to characterize the presence of PVP molecules on the particle surface[44,45] and in order to exclude the effects of free PVP molecules, the Bi_2Se_3 nanosheets are washed three times before undergoing FTIR. The FTIR spectrum in **Figure 2** shows the two characteristic absorption peaks of PVP: a strong absorption band associated with C=O stretching at 1652 cm^{-1} and sharp band arising from C—N stretching at 1286 cm^{-1}.[45] The absorption peaks at 2954 cm^{-1} are assigned to —CH_3 and —CH_2– stretching and that at 3394 cm^{-1} corresponds to —OH stretching of the carbonyl group on the pyrrolyl ring, indicating that the Bi_2Se_3 nanosheets are well dispersed in the aqueous solution.[46] In fact, as shown in Figure 2, the Bi_2Se_3

www.MaterialsViews.com

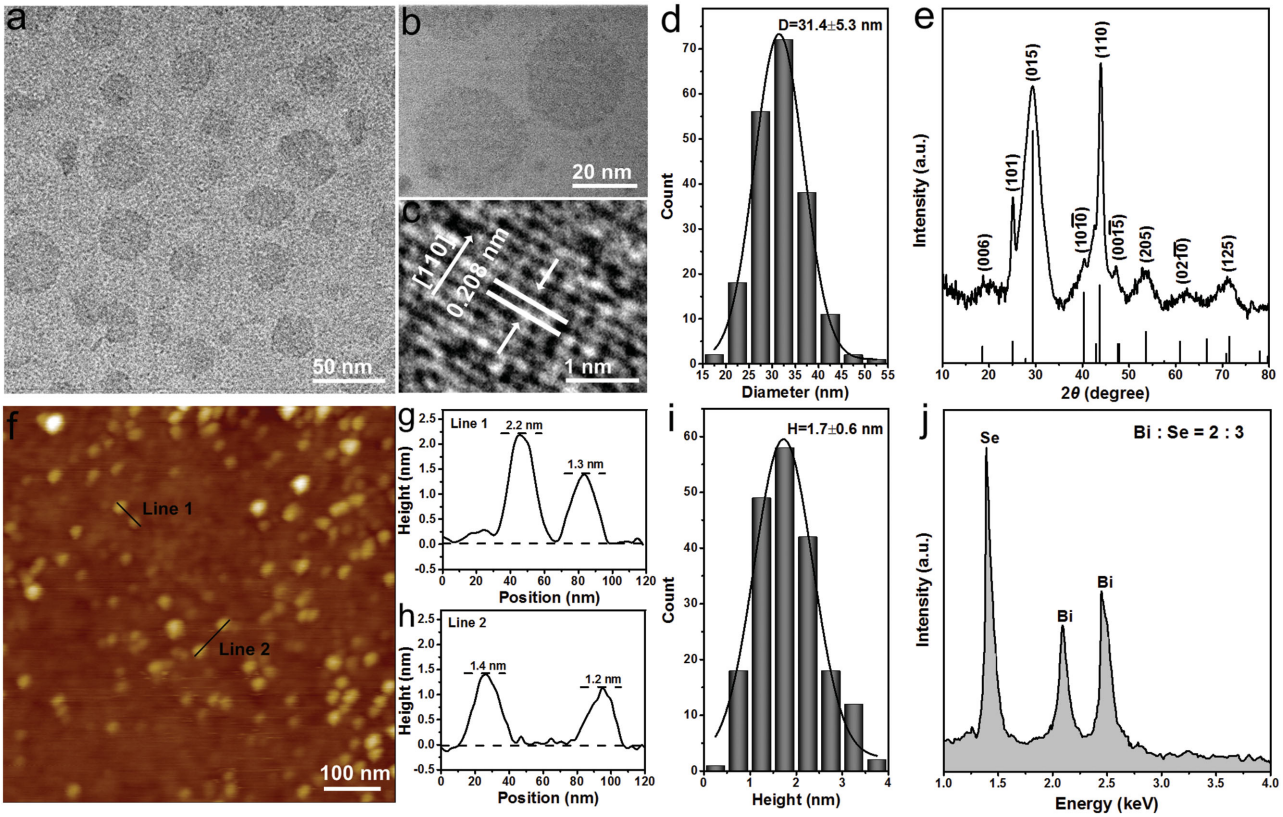

Figure 1. Characterization of Bi_2Se_3 nanosheets: a) TEM image. b) Magnified TEM image. c) HR-TEM image. d) Statistical analysis of lateral diameters of 200 Bi_2Se_3 nanosheets obtained from the TEM images. e) XRD analysis with the black vertical lines being the peaks of bulk Bi_2Se_3 (JCPDS Card No. 33-0214). f) AFM image. g,h) Height profiles along the black lines in (f). i) Statistical analysis of the heights of 200 Bi_2Se_3 nanosheets determined by AFM. j) EDS spectrum.

nanosheets also show good dispersibility in a variety of physiological solutions including phosphate buffered saline (PBS), cell medium (DMEM), and fetal bovine serum (FBS). They also exhibit good stability in these physiological solutions for at least 7 d (see Figure S4, Supporting Information) providing evidence about the favorable surface properties and stability of the PVP-encapsulated Bi_2Se_3 nanosheets boding well for biomedical applications.

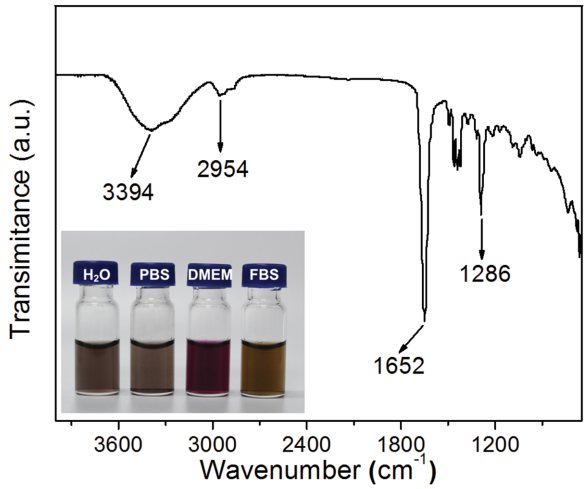

Figure 2. FTIR spectrum of the PVP-encapsulated Bi_2Se_3 nanosheets. Inset: Photograph of the Bi_2Se_3 nanosheets dispersed in various solvents including water, PBS, DMEM, and FBS.

2.2. NIR-Absorption Properties

The NIR absorption properties of the Bi_2Se_3 nanosheets dispersed in the aqueous solution are shown in **Figure 3**a. The optical extinction spectra exhibit a broad absorption band spanning the ultraviolet (UV) and NIR regions similar to other 2D layered materials, such as graphene oxide (GO)[29] and MoS_2.[30] The extinction intensity over the length of the cell (A/L) at λ = 808 nm at different concentrations (C) is determined and the concentration (C) is measured by inductively coupled plasma atomic-emission spectroscopy (ICP-AES). According to Beer's law ($A/L = \alpha C$), the extinction coefficient (α) can be extracted from the slope of the plot of A/L versus concentration (C). The mass extinction coefficient of the Bi_2Se_3 nanosheets is 11.5 L g^{-1} cm^{-1} which is about three times that of Au nanorods (3.9 L g^{-1} cm^{-1}, see Figure 3b and Figure S5, Supporting Information) which are widely used NIR-absorbing agents in PT therapy.[47]

2.3. PT Performance

The NIR PT performance of the Bi_2Se_3 nanosheets is investigated and the results are presented in **Figure 4**. The

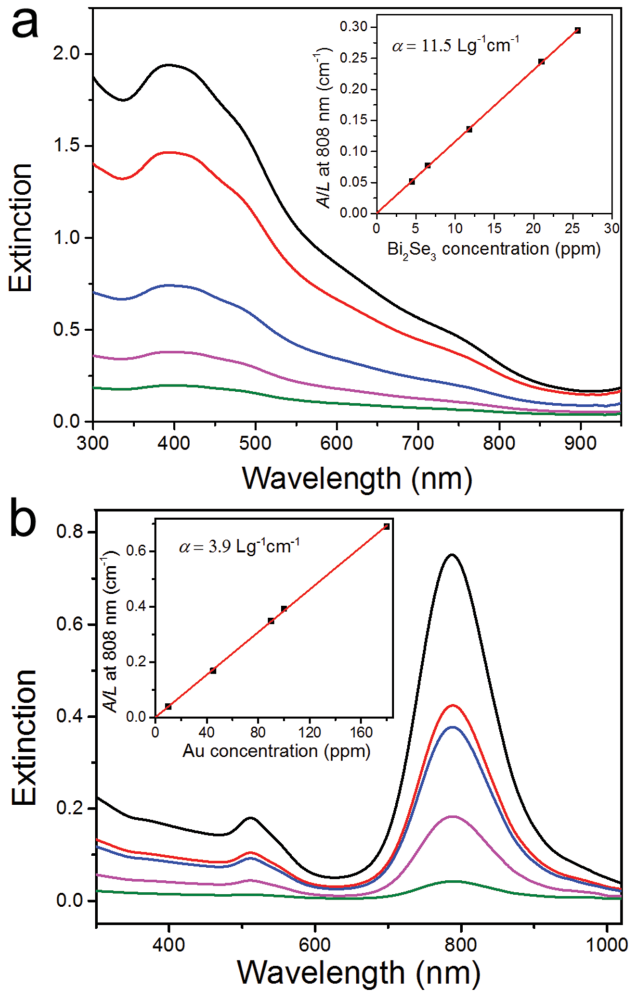

Figure 3. Extinction spectra of a) Bi_2Se_3 nanosheets and b) Au nanorods dispersed in water at different concentrations. Inset: Normalized extinction intensity divided by the characteristic length of the cell (A/L) at different concentrations (C) for $\lambda = 808$ nm.

temperature trends of the aqueous dispersions with different concentrations of Bi_2Se_3 nanosheets (4.7, 11.8, 23.5, 47.0, and 94.0 ppm) are determined by irradiation with an 808 nm NIR laser (1.0 W cm^{-2}) and water was used as the control. As shown in Figure 4a, the temperature rises rapidly with irradiation time. Typically, at a Bi_2Se_3 concentration of 94.0 ppm, the solution temperature increases by 42.5 °C after irradiation for 10 min. In comparison, the temperature of water only increases slightly by only 3.4 °C.

The PT conversion efficiency of the Bi_2Se_3 nanosheets is directly compared with that of Au nanorods (see Figure 4b). Solutions containing 26.1 ppm Bi_2Se_3 nanosheets or 76.9 ppm Au nanorods are prepared to adjust the optical densities at 808 nm to 0.30 (see Figure S6, Supporting Information). The PT heating effects are assessed by irradiating the aqueous dispersion with the 808 nm laser near the plasmon band with a small power density (1.0 W cm^{-2}) for 10 min. After the same laser irradiation, a bigger temperature increase is observed from the solution containing the Bi_2Se_3 nanosheets. By adopting a previously reported method,[48] the PT conversion efficiency of the Bi_2Se_3 nanosheets is determined to be 34.6% which is obviously better than that of the Au nanorods (21.0%).

In order to further assess the PT stability of the Bi_2Se_3 nanosheets, five laser on/off cycles are used. The Bi_2Se_3 nanosheets dispersion is irradiated with the NIR laser for 2 min (Laser on), followed by natural cooling to room temperature after the NIR laser has been turned off (Laser off). The same elevated temperature from different cycles show excellent PT stability of the Bi_2Se_3 nanosheets as no significant decrease can be observed during temperature elevation as shown in Figure 4c. These results indicate that the Bi_2Se_3 nanosheets have good PT conversion efficiency and excellent PT stability boding well for PT therapy.

The PT efficacy of the Bi_2Se_3 nanosheets is examined in vitro. Breast cancer MCF7 cells are incubated with the Bi_2Se_3 nanosheets for 4 h prior to exposure to the NIR laser (808 nm, 1.0 W cm^{-2}) for 10 min. After the PT treatment, calcein AM (live cells, green fluorescence) and propidium iodide (PI; dead cells, red fluorescence) are used to stain the tumor cells to differentiate live/dead cells and then imaged by fluorescence microscopy. As shown in Figure 4d, a Bi_2Se_3-dose-dependent PT effect can be observed from the MCF7 cells. Almost all the cells are killed after incubating with only 50 ppm of the Bi_2Se_3 nanosheets after laser exposure but in contrast, the relative viabilities of the tumor cells in the absence of Bi_2Se_3 nanosheets incubation show little change after the NIR laser illumination. The standard methyl thiazolyl tetrazolium (MTT) assay (Figure 4d) shows similar results. These results clearly indicate the excellent PT efficiency of the Bi_2Se_3 nanosheets in accelerating cancer cell death. It should be emphasized that the concentration of the Bi_2Se_3 nanosheets (50 ppm) and laser power density (1.0 W cm^{-2}) in our experiments are substantially smaller than those adopted in in vitro PT cell destruction by Au nanorods and Au nanocomposites.[49,50] The good PT efficiency of the Bi_2Se_3 nanosheets is likely due to the proper size thus promoting incorporation into the cancer cells.

2.4. PA Imaging

The PT agents with the additional bioimaging ability are highly desirable in imaging-guided PT therapy. **Figure 5**a displays the PA images of the aqueous solutions of the Bi_2Se_3 nanosheets at concentrations between 0 and 250 ppm. A linear relationship of $Y = 11.19 + 4.77X$ between the PA signal intensity and Bi_2Se_3 concentration can be observed ($R^2 = 0.989$) (Figure 5b). Compared to commonly used Au nanorods, these Bi_2Se_3 nanosheets show a much stronger PA signal at the same concentration. For instance, the PA intensity of the 62.5 ppm Bi_2Se_3 nanosheets is 380.2, whereas that of the 250.0 ppm Au nanorods is only 198.4. The PA intensities of the Bi_2Se_3 nanosheets and Au nanorods at the same extinction of 0.51 at 808 nm are compared (see Figure S7, Supporting Information). The PA signal of the Bi_2Se_3 nanosheets is seven times that of Au nanorods providing experimental evidence that the PA conversion ability of the Bi_2Se_3 nanosheets is much better than that of commonly used Au nanorods.

www.MaterialsViews.com

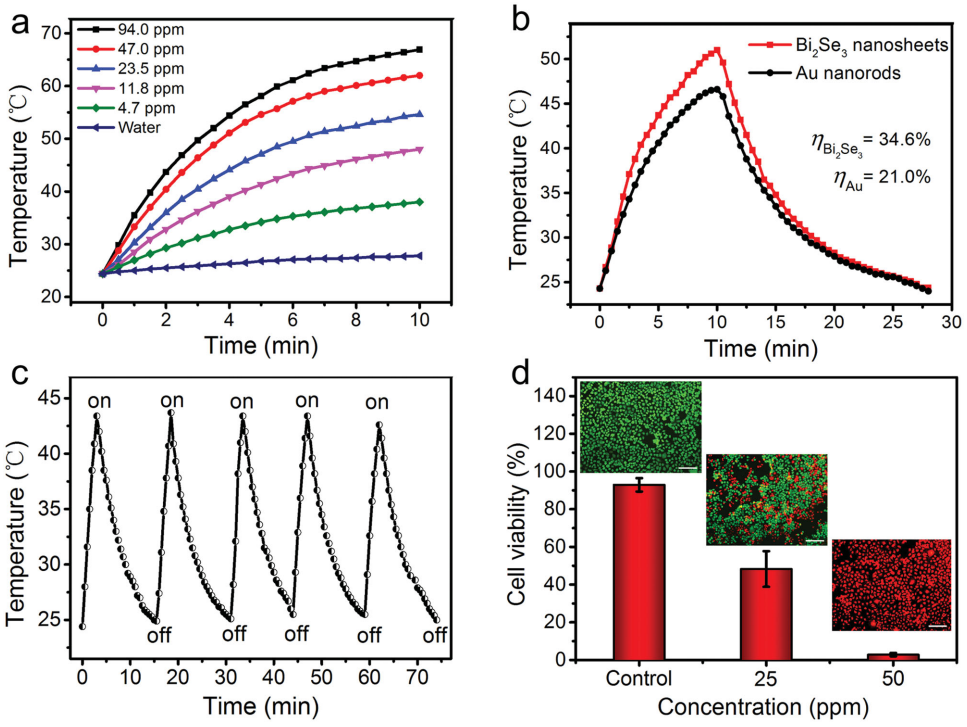

Figure 4. a) PT heating curves of the Bi_2Se_3 nanosheets dispersed in water with a range of concentrations under irradiation with an 808 nm laser (1.0 W cm^{-2}). b) PT heating curve of the aqueous solutions containing 26.1 ppm of the Bi_2Se_3 nanosheets and 76.9 ppm of Au nanorods. c) Temperature variation in the Bi_2Se_3 nanosheets aqueous dispersion during five laser on/off cycles. d) Relative cell viabilities and inset fluorescence images (scale bar = 100 μm) of the MCF7 cells stained with calcein AM (live cells, green fluorescence) and PI (dead cells, red fluorescence) after the different treatments. The standard deviations (SDs) of six parallel samples are used to determine the error bars.

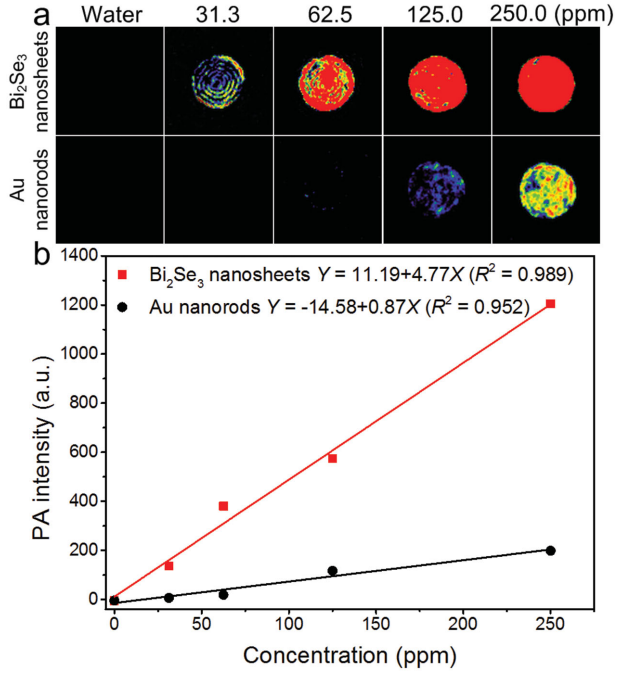

Figure 5. a) PA images of aqueous solutions containing Bi_2Se_3 nanosheets and Au nanorods at different concentrations and b) PA signal intensities of the Bi_2Se_3 nanosheets and Au nanorods as functions of concentrations.

The Bi_2Se_3 nanosheets are subjected to in vivo PA tumor imaging. Balb/c female mice-bearing MCF7 tumors are intravenously injected with 100 μL of the Bi_2Se_3 nanosheets (15.5 mg mL^{-1}) and imaged by a PA imaging system with the 808 nm laser as the excitation source. The final dose in the mice is 103 mg kg^{-1}. PA imaging of the tumor is performed at different time intervals. Before injection, some weak PA signals can be observed from the tumor region due to major blood vasculatures. Within 1 h after intravenous injection of the Bi_2Se_3 nanosheets, the contrast in the tumor is greatly enhanced (**Figure 6**a), indicating gradual accumulation of the Bi_2Se_3 nanosheets in the tumor due to the enhanced EPR effect of cancerous tumors.[51,52] After 5 h, a complete and clear outline of the tumor is obtained from the enhanced PA signal. These results demonstrate that the Bi_2Se_3 nanosheets administered intravenously reach the entire tumor from blood circulation and the PA signals in the tumor last for at least to 72 h (Figure 6b). These results provide strong evidence that the Bi_2Se_3 nanosheets are efficient contrast agents in PA imaging. In addition, the biodistribution of the Bi_2Se_3 nanosheets in the tumor-bearing mice is evaluated 5 h after intravenously postinjection with the Bi_2Se_3 nanosheets (103 mg kg^{-1}) to confirm that the Bi_2Se_3 nanosheets indeed accumulate in the tumor via blood circulation (Figure S8, Supporting Information).

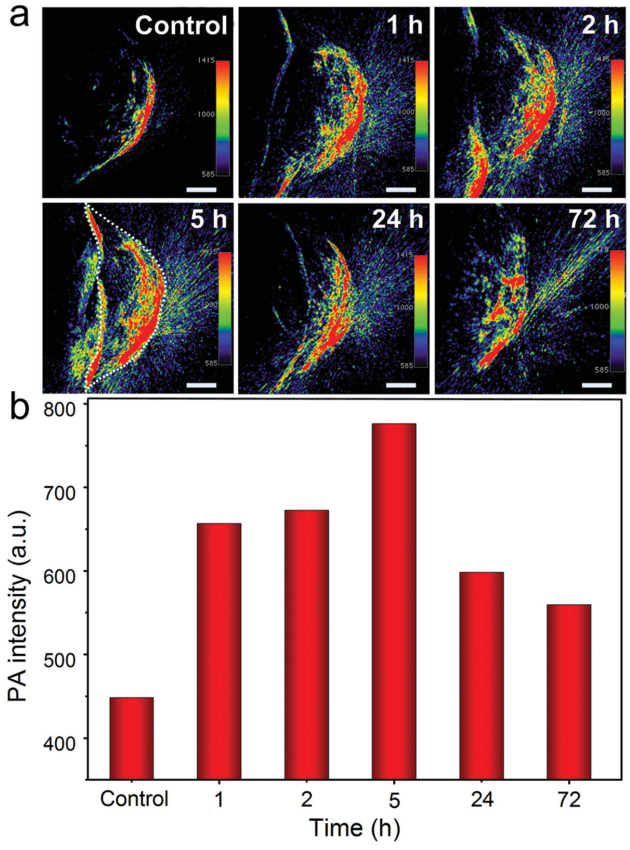

Figure 6. a) PA images of the tumor before and after intravenously injection of Bi_2Se_3 nanosheets at different time intervals (1, 2, 5, 24, and 72 h) with the scale bar = 3 mm and b) PA signal intensities of the tumor at different time after injeciton.

2.5. In Vivo PT Therapy

The in vivo therapeutic efficacy of the Bi_2Se_3 nanosheets is evaluated using MCF7 tumor-bearing nude mice (see **Figure 7**). When the tumors in the mice reach a volume of 150 mm^3, the mice are randomly divided into four groups (n = 5 per group): (a) PBS; (b) PBS + Laser; (c) Bi_2Se_3 nanosheets; (d) Bi_2Se_3 nanosheets + Laser. The MCF7 tumor-bearing nude mice are intravenously injected with Bi_2Se_3 nanosheets (15.5 mg mL^{-1}, 100 µL). According to the PA imaging results, the PT therapy is conducted at 5 h postinjection, at which time point the nanoparticles display the highest tumor accumulation and produce the optimal therapeutic effect. After 5 h postinjection, the tumor-bearing mice are anesthetized and irradiated with NIR light (808 nm, 1.0 W cm^{-2}). The infrared thermal images and temperature changes are recorded on an infrared thermal imaging camera. In the mice intravenously injected with Bi_2Se_3 nanosheets, the tumor surface temperature increases rapidly from 29.9 to 57.4 °C within 10 min of laser irradiation (Figure 7a,b). This temperature is sufficient to kill tumor cells in vivo. For comparison, the tumor temperature of the control group treated with PBS only shows insignificant changes.

The PT therapeutic effect of the Bi_2Se_3 nanosheets is further assessed. The tumor size of each group is determined by a caliper every two days and the results are plotted as a function of time in Figure 7d. In the mice treated with both the Bi_2Se_3 nanosheets and laser irradiation, the tumors shrink gradually and no re-growth is observed, leaving black scars at the initial tumor sites after PT therapy for 14 d (Figure 7c). In contrast, the tumors in the other three groups exhibit rapid tumor growth with time confirming the antitumor efficiency of the Bi_2Se_3 nanosheets in PT therapy.

2.6. Cytotoxicity and In Vivo Acute Toxicity Test

The cytotoxicity of the ultrathin Bi_2Se_3 nanosheets is evaluated by the MTT assay. The MTT assay is performed to determine the relative viability of the MCF7 cells after incubation with Bi_2Se_3 nanosheets at different concentrations between 5 and 200 ppm for 48 h. As shown in **Figure 8**, the cell viability is not compromised by the Bi_2Se_3 nanosheets even when the concentration of the nanosheets is as large as 200 ppm thereby corroborating the low cytotoxicity. To further determine the bio-safety of the Bi_2Se_3 nanosheets in vivo, the acute toxicity test is conducted on the Balb/c mice by intravenous administration of different doses of the Bi_2Se_3 nanosheets from 27 to 1168 mg kg^{-1}. The survival rate of the mice is evaluated 14 d after treatment (Figure S9, Supporting Information). A high dose of the Bi_2Se_3 nanosheets (1168 mg kg^{-1}) causes 100% of mice death within 2 d while a smaller dose of the Bi_2Se_3 nanosheets (900 mg kg^{-1}) causes 20% of mice death within 6 d. However, no death is observed during the period of study if the dose is 750 mg kg^{-1} or less. The mice receiving the 750 mg kg^{-1} of Bi_2Se_3 nanosheets or less do not show any toxic reaction during observation. The acute toxicity test shows that the maximum tolerated dose (MTD) of the Bi_2Se_3 nanosheets is between 750 and 900 mg kg^{-1} and this range is much larger than that commonly used in PT therapy (103 mg kg^{-1}). The results thus confirm that the Bi_2Se_3 nanosheets at the proper concentration have low toxicity. In fact, compared with other inorganic PT materials, such as $Cu_{2-x}S$[53] and MoS_2,[54] the MTD value of these Bi_2Se_3 nanosheets is obviously higher, indicating the Bi_2Se_3 nanosheets are relatively safe and suitable for biomedical applications.

2.7. Biodistribution and Clearance

The long-term toxicity in vivo is always a concern for nanomaterials and it is important to investigate the biodistribution and clearance from the body. 200 µL of the Bi_2Se_3 nanosheets (2 mg mL^{-1}) are intravenously injected into the Balb/c mice. The mice (n = 5 per group) are sacrificed at 1, 5, 10, 15, and 30 d postinjection and the main organs including heart, liver, spleen, lung, and kidney are analyzed for the Bi and Se distributions by ICP-AES. As shown in **Figure 9**a, the Bi_2Se_3 nanosheets mainly accumulate in the liver, spleen, and kidney, whereas the lung and heart show relatively low Bi concentrations. The Bi concentrations drop from 143 µg g^{-1} (liver), 83.2 µg g^{-1} (spleen), and 52.6 µg g^{-1} (kidney) at day 1 to only 14.8 µg g^{-1} (liver), 10.4 µg g^{-1} (spleen), and 8.6 µg g^{-1} (kidney) at day 30. Not surprisingly, Se is also detected mainly

www.MaterialsViews.com

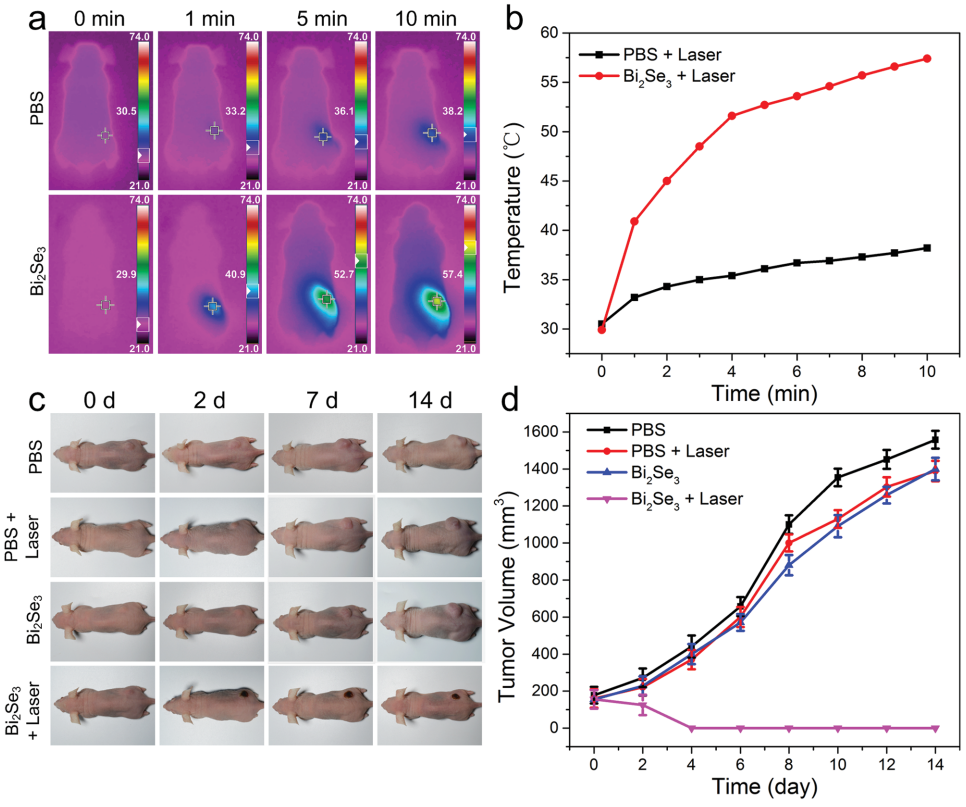

Figure 7. a) Infrared thermal images and b) time-dependent temperature increase in the MCF7 tumor-bearing nude mice under 808 nm light irradiation 5 h after intravenous injection of PBS and Bi_2Se_3 nanosheets. c) Photographs of the mice after the treatment for 0, 2, 7, and 14 d, and d) growth of MCF7 tumors in different groups after the treatment.

from the liver, spleen, and kidney but less from the lung and heart (Figure 9b). At day 1, the Se concentrations are 29.8 μg g^{-1} (liver), 24.4 μg g^{-1} (spleen), and 16.7 μg g^{-1} (kidney) but decrease to 3.7 μg g^{-1} (liver), 3.4 μg g^{-1} (spleen), and 2.8 μg g^{-1} (kidney) at day 30. Both the Bi and Se concentrations decrease with time indicating time-dependent clearance effects. The liver and spleen are dominant from the viewpoint of accumulation of the nanosheets mainly due to reticuloendothelial system (RES) absorption. The Bi concentration is larger than that of Se and the mismatch before and after injection is because the Bi_2Se_3 nanosheets are oxidized in air.[25]

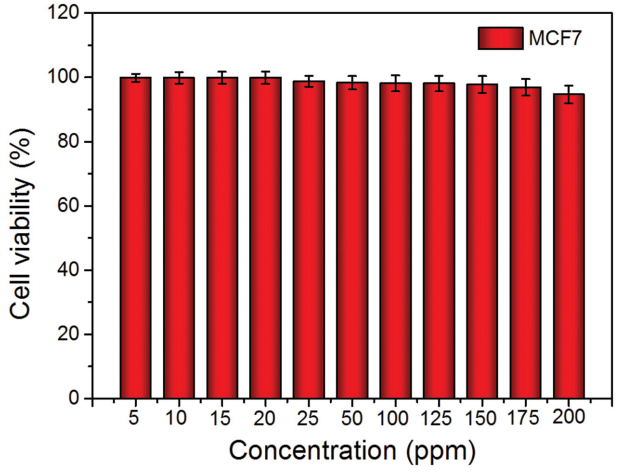

Figure 8. Relative viabilities of MCF7 cells after incubation with various concentrations (5–200 ppm) of Bi_2Se_3 nanosheets at 37 °C for 48 h.

To further investigate the clearance efficiency in details, the time-dependent residual amounts in the mice treated with the Bi_2Se_3 nanosheets are determined (Figure 9c,d). The residual Bi and Se in all the organs are summed. The original total amounts of Bi and Se are 255.2 and 144.8 μg, respectively, and the residual ratios of Bi and Se are calculated by normalizing the residual amounts to initial total amounts. The residual amount of Bi in the mice is 205.8 μg at day 1 and decreases to 36.1 μg at day 30. The corresponding residual ratio of Bi decreases from 80.6% at day 1 to 14.1% at day 30. Similarly, the residual amount of Se in the mice is 46.9 μg at day 1 and decreases to 9.9 μg at day 30, whereas the calculated residual ratio of Se decreases from 32.0% at day 1 to only 6.8% at day 30. These results suggest that the ultrathin Bi_2Se_3 nanosheets are metabolizable and the clearance efficiency is obviously higher than that of bigger Bi_2Se_3 nanosheets.[25]

3. Conclusion

The PVP-encapsulated Bi_2Se_3 nanosheets with a thickness of 1.7 nm and diameter of 31.4 nm are synthesized by a "green" solution-based method and used as an efficient NIR-triggered theranostic agent. Possessing an extinction coefficient of 11.5 L g^{-1} cm^{-1} at 808 nm, the ultrathin Bi_2Se_3 nanosheets boast a high PT conversion efficiency of 34.6%

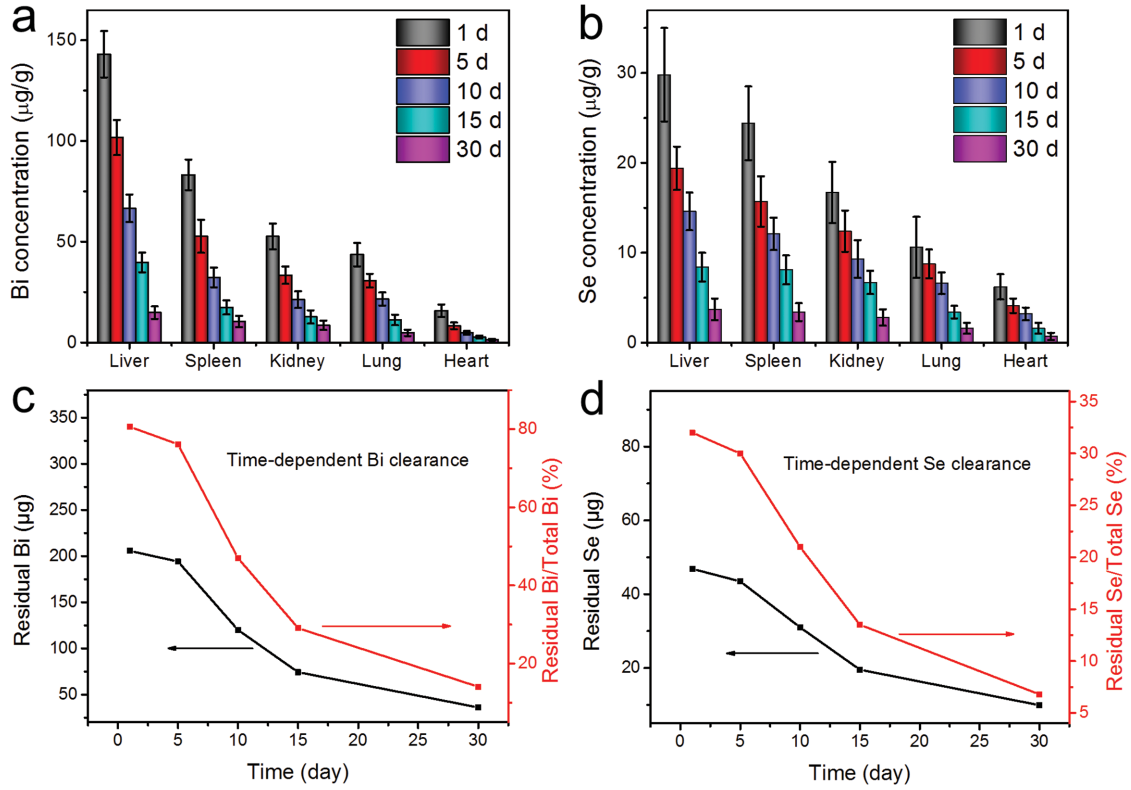

Figure 9. In vivo biodistribution and clearance of the Bi_2Se_3 nanosheets in different organs: a) Bi concentrations and b) Se concentrations at different time points of 1, 5, 10, 15, and 30 d after intravenous injection (20 mg kg^{-1}). The residual amounts and corresponding residual ratios of c) Bi and d) Se plotted versus time after intravenous injection of the Bi_2Se_3 nanosheets.

and also deliver excellent PA performance. After systemic administration, the Bi_2Se_3 nanosheets not only accumulate passively in the entire tumors enabling efficient PA imaging-guided PT therapy, but also are excreted from the body efficiently within one month. These attractive properties render the ultrathin Bi_2Se_3 nanosheets promising as NIR-triggered theranostic agents in cancer therapies.

4. Experimental Section

Materials: The selenium powders (Se, 99.0%), acetone (≥99.8%), and ethylene glycol (EG, ≥99.0%) were obtained from Sinopharm Chemical Reagent Co. Ltd. (Shanghai, China). Sodium borohydride ($NaBH_4$, 96.0%), bismuth nitrate pentahydrate ($Bi(NO_3)_3{\cdot}5H_2O$, 99.99+%), and PVP ($M_w \approx 55\,000$) were purchased from Sigma-Aldrich. All the chemicals were analytical reagent grade and used without further purification. Ultrapure water (18.25 MΩ cm, 25 °C) was used in the experiments.

Synthesis of Ultrathin Bi_2Se_3 Nanosheets: The NaHSe aqueous solution was produced by reacting $NaBH_4$ with Se powders with a molar ratio of 2:1 in an ice-water bath. The transparent solution was sealed for the following reaction. The Bi_2Se_3 nanosheets were prepared by the reaction between $Bi(NO_3)_3{\cdot}5H_2O$ and the NaHSe solution as shown in the following. 0.5 g of PVP were dissolved in 20 mL of EG and the solution was poured into a 100 mL round-bottom flask, followed by addition of a solution of $Bi(NO_3)_3{\cdot}5H_2O$ (0.226 g in 12.5 mL of EG) under magnetic stirring at room temperature. The flask was sealed and heated to 160 °C under N_2. As the temperature went up, the transparent mixture became yellow and then turned turbid at 160 °C. The freshly synthesized oxygen-free NaHSe solution (0.667 mol L^{-1}, 1.048 mL) was rapidly injected into the mixture by a syringe. The mixture turned dark immediately as a result of the formation of PVP-encapsulated Bi_2Se_3 nanosheets. The reaction proceeded for 10 min before cooling to room temperature. The products were precipitated by centrifuging (12 000 rpm, 10 min) and washed three times with a mixture of acetone (400 mL) and ultrapure water (80 mL).

Characterization: TEM was performed on the Tecnai G2 F20 S-Twin transmission electron microscope at an acceleration voltage of 200 kV. AFM was carried out on the drop-cast flakes on Si/SiO_2 substrates on the MFP-3D-S atomic force microscope (Asylum Research, USA) using the AC mode (tapping mode) in air. EDS was conducted on the Oxford INCA 300. Raman scattering was carried out on a Horiba Jobin-Yvon Lab Ram HR VIS high-resolution confocal Raman microscope, XPS was conducted on the Thermo Fisher ESCALAB 250Xi XPS, and FTIR was performed on a Nicolet, CCR-1 FTIR spectrometer at room temperature. The UV–vis–NIR extinction spectra were acquired on a Lambda25 spectrophotometer (PerkinElmer) with QS-grade quartz cuvettes at room temperature. The Bi_2Se_3 concentration was determined by ICP-AES (7000DV, PerkinElmer). Using Beer's law ($A/L = \alpha C$), the Bi_2Se_3 nanosheets extinction coefficient was extracted from the slope of a plot of A/L versus concentration (C). The optical extinction per cell length (A/L) was determined from the optical extinction intensity at 808 nm.

PT Heating Experiments: A fiber-coupled continuous semiconductor diode laser (808 nm, KS-810F-8000, Kai Site Electronic Technology Co., Ltd. Shaanxi, China) with a power density of

1.0 W cm^{-2} was used in the experiments. To study the PT effect, a 1 cm quartz cuvette containing 1 mL of the sample was clamped onto the top part above the sample surface and the bottom of the cuvette was kept at about 0.5 cm above the magnetic stirrer. The measurement was conducted by irradiating the well for 10 min and simultaneously monitoring the solution temperature using an infrared thermal imaging camera (Fluke Ti27, USA).

In Vitro PT Therapy: To study the PT therapeutic effects of Bi_2Se_3 nanosheets, the MCF7 cells (1×10^4 cells per well) were seeded on 96-well plates and incubated in a humidified 5% CO_2 atmosphere overnight at 37 °C. The MCF7 cells were cultured with and without the Bi_2Se_3 nanosheets (25, 50 ppm) for 4 h at 37 °C under the same conditions and then illuminated by an 808 nm laser with a power density of 1.0 W cm^{-2} for 10 min. The laser spot was adjusted to fully cover the area of each well. After irradiation, the samples were incubated at 37 °C in 5% CO_2 and 95% air humidified atmosphere for 12 h. The treated cells were rinsed with PBS, co-stained with Calcein AM and PI for 30 min, and then imaged with an Olympus IX71 motorized inverted microscope.

PA Imaging: To analyze the contrast efficacy, the PA images in vitro and in vivo were obtained on a PA computed tomography scanner (Endra Nexus 128, USA). In in vitro PA imaging, the ultrathin Bi_2Se_3 nanosheets and Au nanorods were dispersed in water at different concentrations from 0 to 250 ppm and irradiated with the 808 nm laser. In in vivo PA imaging, 100 µL of the ultrathin Bi_2Se_3 nanosheets suspension with a concentration of 15.5 mg mL^{-1} was intravenously administered by subcutaneous injection into the tumor-bearing Balb/c nude mice. The mice was anesthetized by intraperitoneal injection of sodium pentobarbital and the temperature of the mice body was maintained by using a water heating system at 37.5 °C. PA scanning was performed before and after intravenous injection with the ultrathin Bi_2Se_3 nanosheets at different time intervals (1, 2, 5, 24, and 72 h). All the PA scans were conducted at the 808 nm laser wavelength.

In Vivo PT Therapy: The MCF7 cells (1×10^6 cells in 100 µL PBS) were subcutaneously injected into the right leg of the mice. When the tumor size reached about 150 mm^3, the mice were divided into four groups (n = 5 per group): (a) PBS; (b) PBS + Laser; (c) Bi_2Se_3 nanosheets; (d) Bi_2Se_3 nanosheets + Laser. The MCF7 tumor-bearing nude mice were intravenously injected with Bi_2Se_3 nanosheets (15.5 mg mL^{-1}, 100 µL). After 5 h postinjection, the tumor-bearing mice were anesthetized by injection of sodium pentobarbital and exposed to NIR light (808 nm, 1.0 W cm^{-2}) for 10 min. The infrared thermal images and temperature changes were monitored by an infrared thermal imaging camera. The images were recorded at 0, 1, 5, and 10 min. The tumor sizes were measured by a caliper every two days after the treatment and no mice died during the course of therapy.

Cytotoxicity Test: The MCF7 cells were cultured at 37 °C in a humidified atmosphere with 5% CO_2 and on a 96-well plate (1×10^4 cells per well) in Dulbecco's Modified Eagle medium (Gibco BRL) supplemented with 10% (v/v) fetal bovine serum, 100 UI mL^{-1} penicillin, and 100 UI mL^{-1} streptomycin. After 12 h, the DMEM was replaced with 200 µL of the DMEM medium that contained 20 µL per well of Bi_2Se_3 nanosheets with a series concentrations of 5–200 ppm, respectively. The cells were incubated with the samples for 48 h. The effects of different concentrations of Bi_2Se_3 nanosheets were determined by MTT. The MTT reagent was dispersed in the PBS solution with a concentration of 5 mg mL^{-1} and filtered by a 0.22×10^{-6} M filter to disinfect and eliminate insoluble residues and then stored in amber vials at 4 °C. The cell viability was assessed by adding 20 µL of the MTT PBS solution (5 mg mL^{-1}) to each well. After treatment with MTT at 37 °C for 4 h, the MTT solution was removed and the medium was replaced with 200 µL of dimethyl sulfoxide (DMSO) to dissolve the formazan crystals. A Thermo Reader at test wavelength of 490 nm was employed to measure the optical absorbance of each well which was correlated with the number of viable cells. The following formula was used to calculate the inhibition of cell growth: Cell viability (%) = (Mean of absolute value of treatment group/mean absolute value of control) × 100%.

Biodistribution: The Bi_2Se_3 nanosheets were injected into the Balb/c mice (20 mg kg^{-1}) via the tail vein. After 1, 5, 10, 15, and 30 d postinjection, the mice were euthanized and the tissues were excised, weighed, and digested in HNO_3 (65%) for 24 h. The homogenized tissue lysates were dried by heat, diluted with ultrapure water, and filtered. The Bi and Se contents were determined by ICP-AES.

All animal experiments were performed in accordance with guidelines evaluated and approved by the Animal Care and Use Committee of the Shenzhen Institutes of Advanced Technology, Chinese Academy of Sciences.

Supporting Information

Supporting Information is available from the Wiley Online Library or from the author.

Acknowledgements

The authors gratefully acknowledge financial support from the Science and Technology Key Projects of Shenzhen (JCYJ20140417113430608 and JCYJ20150401145529032) and Hong Kong Research Grants Council (RGC) General Research Funds (GRF) No. CityU 11301215.

[1] T. S. Hauck, T. L. Jennings, T. Yatsenko, J. C. Kumaradas, W. C. W. Chan, *Adv. Mater.* **2008**, *20*, 3832.
[2] Y. Sang, Z. Zhao, M. Zhao, P. Hao, Y. Leng, H. Liu, *Adv. Mater.* **2015**, *27*, 363.
[3] X. R. Song, X. Wang, S. X. Yu, J. Cao, S. H. Li, J. Li, G. Liu, H. H. Yang, X. Chen, *Adv. Mater.* **2015**, *27*, 3285.
[4] Z. Li, Y. Hu, K. A. Howard, T. Jiang, X. Fan, Z. Miao, Y. Sun, F. Besenbacher, M. Yu, *ACS Nano* **2016**, *10*, 984.
[5] Z. Li, H. Huang, S. Tang, Y. Li, X. F. Yu, H. Wang, P. Li, Z. Sun, H. Zhang, C. Liu, P. K. Chu, *Biomaterials* **2016**, *74*, 144.
[6] B. Wang, J. H. Wang, Q. Liu, H. Huang, M. Chen, K. Li, C. Li, X. F. Yu, P. K. Chu, *Biomaterials* **2014**, *35*, 1954.
[7] W. Yin, L. Yan, J. Yu, G. Tian, L. Zhou, X. Zheng, X. Zhang, Y. Yong, J. Li, Z. Gu, Y. Zhao, *ACS Nano* **2014**, *8*, 6922.
[8] M. S. Yavuz, Y. Cheng, J. Chen, C. M. Cobley, Q. Zhang, M. Rycenga, J. Xie, C. Kim, K. H. Song, A. G. Schwartz, L. V. Wang, Y. Xia, *Nat. Mater.* **2009**, *8*, 935.

[9] O. Akhavan, E. Ghaderi, *Small* **2013**, *9*, 3593.
[10] S. Tang, M. Chen, N. Zheng, *Small* **2014**, *10*, 3139.
[11] K. Yang, L. Feng, X. Shi, Z. Liu, *Chem. Soc. Rev.* **2013**, *42*, 530.
[12] J. W. Kim, E. I. Galanzha, E. V. Shashkov, H. M. Moon, V. P. Zharov, *Nat. Nanotechnol.* **2009**, *4*, 688.
[13] X. Liang, Y. Li, X. Li, L. Jing, Z. Deng, X. Yue, C. Li, Z. Dai, *Adv. Funct. Mater.* **2015**, *25*, 1451.
[14] W. Li, P. Rong, K. Yang, P. Huang, K. Sun, X. Chen, *Biomaterials* **2015**, *45*, 18.
[15] X. Yi, K. Yang, C. Liang, X. Zhong, P. Ning, G. Song, D. Wang, C. Ge, C. Chen, Z. Chai, Z. Liu, *Adv. Funct. Mater.* **2015**, *25*, 4689.
[16] K. Yang, L. Hu, X. Ma, S. Ye, L. Cheng, X. Shi, C. Li, Y. Li, Z. Liu, *Adv. Mater.* **2012**, *24*, 1868.
[17] L. Cheng, S. Shen, S. Shi, Y. Yi, X. Wang, G. Song, K. Yang, G. Liu, T. E. Barnhart, W. Cai, Z. Liu, *Adv. Funct. Mater.* **2016**, *26*, 2185.
[18] J. Liu, X. Zheng, L. Yan, L. Zhou, G. Tian, W. Yin, L. Wang, Y. Liu, Z. Hu, Z. Gu, C. Chen, Y. Zhao, *ACS Nano* **2015**, *9*, 696.
[19] G. Song, C. Liang, H. Gong, M. Li, X. Zheng, L. Cheng, K. Yang, X. Jiang, Z. Liu, *Adv. Mater.* **2015**, *27*, 6110.
[20] A. K. Geim, *Science* **2009**, *324*, 1530.
[21] J. N. Coleman, M. Lotya, A. O'Neill, S. D. Bergin, P. J. King, U. Khan, K. Young, A. Gaucher, S. De, R. J. Smith, *Science* **2011**, *331*, 568.
[22] D. Voiry, H. Yamaguchi, J. Li, R. Silva, D. C. B. Alves, T. Fujita, M. Chen, T. Asefa, V. B. Shenoy, G. Eda, M. Chhowalla, *Nat. Mater.* **2013**, *12*, 850.
[23] Z. Zeng, T. Sun, J. Zhu, X. Huang, Z. Yin, G. Lu, Z. Fan, Q. Yan, H. H. Hng, H. Zhang, *Angew. Chem. Int. Ed.* **2012**, *51*, 9052.
[24] S. S. Chou, B. Kaehr, J. Kim, B. M. Foley, M. De, P. E. Hopkins, J. Huang, C. J. Brinker, V. P. Dravid, *Angew. Chem. Int. Ed.* **2013**, *52*, 4160.
[25] X. D. Zhang, J. Chen, Y. Min, G. B. Park, X. Shen, S. S. Song, Y. M. Sun, H. Wang, W. Long, J. Xie, K. Gao, L. Zhang, S. Fan, F. Fan, U. Jeong, *Adv. Funct. Mater.* **2014**, *24*, 1718.
[26] J. Li, F. Jiang, B. Yang, X. R. Song, Y. Liu, H. H. Yang, D. R. Cao, W. R. Shi, G. N. Chen, *Sci. Rep.* **2013**, *3*, 1998.
[27] L. Cheng, J. Liu, X. Gu, H. Gong, X. Shi, T. Liu, C. Wang, X. Wang, G. Liu, H. Xing, W. Bu, B. Sun, Z. Liu, *Adv. Mater.* **2014**, *26*, 1886.
[28] T. Liu, C. Wang, X. Gu, H. Gong, L. Cheng, X. Shi, L. Feng, B. Sun, Z. Liu, *Adv. Mater.* **2014**, *26*, 3433.
[29] J. T. Robinson, S. M. Tabakman, Y. Liang, H. Wang, H. S. Casalongue, D. Vinh, H. Dai, *J. Am. Chem. Soc.* **2011**, *133*, 6825.
[30] T. Liu, S. Shi, C. Liang, S. Shen, L. Cheng, C. Wang, X. Song, S. Goel, T. E. Barnhart, W. Cai, Z. Liu, *ACS Nano* **2015**, *9*, 950.
[31] H. Zhang, C. X. Liu, X. L. Qi, X. Dai, Z. Fang, S. C. Zhang, *Nat. Phys.* **2009**, *5*, 438.
[32] M. X. Wang, C. Liu, J. P. Xu, F. Yang, L. Miao, M. Y. Yao, C. L. Gao, C. Shen, X. Ma, X. Chen, Z. A. Xu, Y. Liu, S. C. Zhang, D. Qian, J. F. Jia, Q. K. Xue, *Science* **2012**, *336*, 52.
[33] H. Peng, W. Dang, J. Cao, Y. Chen, D. Wu, W. Zheng, H. Li, Z. X. Shen, Z. Liu, *Nat. Chem.* **2012**, *4*, 281.
[34] A. Zhuang, J. J. Li, Y. C. Wang, X. Wen, Y. Lin, B. Xiang, X. Wang, J. Zeng, *Angew. Chem.* **2014**, *126*, 6543.
[35] O. Rabin, J. M. Perez, J. Grimm, G. Wojtkiewicz, R. Weissleder, *Nat. Mater.* **2006**, *5*, 118.
[36] J. M. Kinsella, R. E. Jimenez, P. P. Karmali, A. M. Rush, V. R. Kotamraju, N. C. Gianneschi, E. Ruoslahti, D. Stupack, M. J. Sailor, *Angew. Chem. Int. Ed.* **2011**, *50*, 12308.
[37] K. Ai, Y. Liu, J. Liu, Q. Yuan, Y. He, L. Lu, *Adv. Mater.* **2011**, *23*, 4886.
[38] P. D. Whanger, *Br. J. Nutr.* **2004**, *91*, 11.
[39] Y. Min, G. D. Moon, B. S. Kim, B. Lim, J. S. Kim, C. Y. Kang, U. Jeong, *J. Am. Chem. Soc.* **2012**, *134*, 2872.
[40] L. Sun, Z. Lin, J. Peng, J. Weng, Y. Huang, Z. Luo, *Sci. Rep.* **2014**, *4*, 4794.
[41] K. J. Koski, J. J. Cha, B. W. Reed, C. D. Wessells, D. Kong, Y. Cui, *J. Am. Chem. Soc.* **2012**, *134*, 7584.
[42] M. K. Jana, K. Biswas, C. N. R. Rao, *Chem. Eur. J.* **2013**, *19*, 9110.
[43] D. Kong, J. J. Cha, K. Lai, H. Peng, J. G. Analytis, S. Meister, Y. Chen, H. J. Zhang, I. R. Fisher, Z. X. Shen, Y. Cui, *ACS Nano* **2011**, *5*, 4698.
[44] H. Wang, X. Qiao, J. Chen, X. Wang, S. Ding, *Mater. Chem. Phys.* **2005**, *94*, 449.
[45] H. L. Liu, P. Hou, W. X. Zhang, J. H. Wu, *Colloids Surf. A: Physicochem. Eng. Aspects* **2010**, *356*, 21.
[46] X. Zhang, N. Sun, B. Wu, Y. Lu, T. Guan, W. Wu, *Powder Technol.* **2008**, *182*, 480.
[47] X. Yang, M. Yang, B. Pang, M. Vara, Y. Xia, *Chem. Rev.* **2015**, *115*, 10410.
[48] Q. Tian, F. Jiang, R. Zou, Q. Liu, Z. Chen, M. Zhu, S. Yang, J. Wang, J. Wang, J. Hu, *ACS Nano* **2011**, *5*, 9761.
[49] X. Huang, I. H. El-Sayed, W. Qian, M. A. El-Sayed, *J. Am. Chem. Soc.* **2006**, *128*, 2115.
[50] H. Ke, X. Yue, J. Wang, S. Xing, Q. Zhang, Z. Dai, J. Tian, S. Wang, Y. Jin, *Small* **2014**, *10*, 1220.
[51] L. Cheng, K. Yang, Q. Chen, Z. Liu, *ACS Nano* **2012**, *6*, 5605.
[52] K. Yang, S. Zhang, G. Zhang, X. Sun, S. T. Lee, Z. Liu, *Nano Lett.* **2010**, *10*, 3318.
[53] S. Wang, A. Riedinger, H. Li, C. Fu, H. Liu, L. Li, T. Liu, L. Tan, M. J. Barthel, G. Pugliese, F. D. Donato, M. S. D'Abbusco, X. Meng, L. Manna, H. Meng, T. Pellegrino, *ACS Nano* **2015**, *9*, 1788.
[54] S. Wang, L. Tan, P. Liang, T. Liu, J. Wang, C. Fu, J. Yu, J. Dou, H. Li, X. Meng, *J. Mater. Chem. B* **2016**, *4*, 2133.

Received: March 28, 2016
Revised: May 9, 2016
Published online: June 22, 2016